Journal of the Physical Society of Japan **92**, 034803 (2023)
https://doi.org/10.7566/JPSJ.92.034803

Simulations of Odd Microswimmers

Akira Kobayashi[1], Kento Yasuda[2], Li-Shing Lin[1], Isamu Sou[1], Yuto Hosaka[3], and Shigeyuki Komura[4,5,1*]

[1]*Department of Chemistry, Graduate School of Science, Tokyo Metropolitan University, Hachioji, Tokyo 192-0397, Japan*
[2]*Research Institute for Mathematical Sciences, Kyoto University, Kyoto 606-8502, Japan*
[3]*Max Planck Institute for Dynamics and Self-Organization (MPI DS), Am Fassberg 17, 37077 Göttingen, Germany*
[4]*Wenzhou Institute, University of Chinese Academy of Sciences, Wenzhou, Zhejiang 325001, China*
[5]*Oujiang Laboratory, Wenzhou, Zhejiang 325000, China*

(Received October 24, 2022; revised January 6, 2023; accepted January 20, 2023; published online February 21, 2023)

We perform numerical simulations of odd microswimmers consisting of three spheres and two odd springs. To describe the hydrodynamic interaction, both the Oseen-type and the Rotne–Prager–Yamakawa (RPY)-type mobilities are used. For the Oseen-type mobility, the simulation results quantitatively reproduce the asymptotic expression of the average velocity. For the RPY-type mobility, on the other hand, the average velocity is smaller than that of the Oseen-type mobility and the deviation is more pronounced for larger spheres. We also perform simulations of microswimmers having different sphere sizes and show that the average velocity becomes smaller than that of the equal size case. The size of the middle sphere plays an important role in determining the average velocity.

1. Introduction

Recently, Scheibner et al. introduced the concept of odd elasticity that is useful to characterize nonequilibrium active systems.[1,2] Odd elasticity arises from antisymmetric (odd) components of the elastic modulus tensor that violates the energy conservation law and thus can exist only in active materials[3] or biological systems.[4] Unlike passive materials, a finite amount of work can be extracted in odd elastic systems through quasi-static cycle of deformations.[1,2] It was also shown that antisymmetric parts of the time-correlation functions in odd Langevin systems are proportional to the odd elasticity.[5] The concept of odd elasticity can be further extended to quantify the nonreciprocality of active micromachines (such as enzymes or motor proteins) and microswimmers.[6,7] According to Purcell's scallop theorem for microswimmers,[8] nonreciprocal body motion is required for locomotion in a Newtonian fluid. Within the Onsager's variational principle,[9] it was shown that odd elastic moduli are proportional to the nonequilibrium force.[10]

Moreover, we have proposed a model of a thermally driven microswimmer in which three spheres are connected by two springs having odd elasticity.[11] It was theoretically shown that the presence of odd elasticity leads to a directional locomotion of the stochastic microswimmer. We have analytically obtained the average velocity under the assumption that the sphere size and the spring extensions are small enough compared to the natural length of the spring. As we show later again, the average velocity is proportional to the odd elastic constant whose sign determines the swimming direction.

In this paper, we report the results of numerical simulations of odd microswimmers to check the validity of our analytical prediction.[11] For comparison, we use both the Oseen-type and the Rotne–Prager–Yamakawa (RPY)-type hydrodynamic mobilities in our simulations.[12,13] To numerically integrate the multiplicative Langevin equations, we also employ the previously suggested formulation that assures the equilibrium distribution.[14,15] Although our previous work considered only the case when the sphere size is identical,[11] we also perform the simulations for odd microswimmers having different sphere sizes.

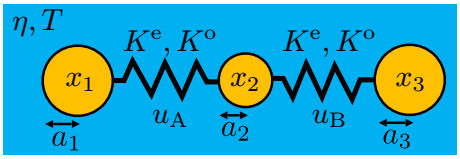

Fig. 1. (Color online) Odd microswimmer in a fluid with viscosity η and temperature T. Three spheres of radius a_i $(i = 1, 2, 3)$ are connected by two springs with natural length ℓ. Each spring has both even elastic constant K^{e} and odd elastic constant K^{o}.

2. Model

Let us first review the model of an odd microswimmer.[11] As depicted in Fig. 1, we consider a three-sphere microswimmer in which the positions of the three spheres of radius a_i are given by x_i $(i = 1, 2, 3)$ in a one-dimensional coordinate system.[16,17] These three spheres are connected by two springs that exhibit both even and odd elasticities.[1,2] We denote the two spring extensions by $u_{\mathrm{A}} = x_2 - x_1 - \ell$ and $u_{\mathrm{B}} = x_3 - x_2 - \ell$, where ℓ is the natural length. Then the forces F_{A} and F_{B} conjugate to u_{A} and u_{B}, respectively, are given by $F_\alpha = -K_{\alpha\beta}u_\beta$ $(\alpha, \beta = \mathrm{A}, \mathrm{B})$. For an odd spring, the elastic constant $K_{\alpha\beta}$ is given by[5–7,11]

$$K_{\alpha\beta} = K^{\mathrm{e}}\delta_{\alpha\beta} + K^{\mathrm{o}}\epsilon_{\alpha\beta}, \tag{1}$$

where K^{e} and K^{o} are even and odd elastic constants in the two-dimensional configuration space, $\delta_{\alpha\beta}$ is the Kronecker delta, and $\epsilon_{\alpha\beta}$ is the 2D Levi-Civita tensor. The forces f_i acting on each sphere are given by $f_1 = -F_{\mathrm{A}}, f_2 = F_{\mathrm{A}} - F_{\mathrm{B}}$, and $f_3 = F_{\mathrm{B}}$. We note that these forces satisfy the force-free condition, i.e., $f_1 + f_2 + f_3 = 0$.

The above odd microswimmer is immersed in a fluid of shear viscosity η and temperature T. Then the Langevin equation of each sphere is given by

$$\dot{x}_i = M_{ij}f_j + \xi_i, \tag{2}$$

where $\dot{x}_i = dx_i/dt$ and M_{ij} are the hydrodynamic mobility coefficients. In the previous work, we used the Oseen-type mobility[11]

$$M_{ij}^{\mathrm{O}} = \begin{cases} 1/(6\pi\eta a_i) & (i=j) \\ 1/(4\pi\eta|x_i - x_j|) & (i \neq j) \end{cases}. \tag{3}$$

The Gaussian white-noise sources ξ_i have zero mean, $\langle \xi_i(t) \rangle = 0$, and their correlations satisfy the fluctuation-dissipation theorem $\langle \xi_i(t)\xi_j(t') \rangle = 2k_{\mathrm{B}}TM_{ij}^{\mathrm{O}}\delta(t-t')$, where k_{B} is the Boltzmann constant. The total velocity of the microswimmer is given by $V = (\dot{x}_1 + \dot{x}_2 + \dot{x}_3)/3$.

When all the spheres have the same radius a, the average velocity was obtained in the limit of $u_{\mathrm{A}}, u_{\mathrm{B}} \ll \ell$ and $a \ll \ell$ as[11]

$$\langle V \rangle \approx \frac{7k_{\mathrm{B}}T\lambda}{48\pi\eta\ell^2}, \tag{4}$$

where $\lambda = K^{\mathrm{o}}/K^{\mathrm{e}}$. As discussed in Ref. 1, $\langle V \rangle$ in Eq. (4) is the product of the geometrical factor, the explored area in the configuration space, and the speed of the rotational probability flux.

In the current simulation study, we also use the RPY-type mobility that takes into account the next-higher order term in the far-field approximation:[12,13]

$$M_{ij}^{\mathrm{RPY}} = \begin{cases} 1/(6\pi\eta a_i) & (i=j) \\ \dfrac{1}{4\pi\eta|x_i - x_j|}\left(1 - \dfrac{a_i^2 + a_j^2}{3|x_i - x_j|^2}\right) & \\ \qquad (i \neq j \text{ and } |x_i - x_j| \geq a_i + a_j) & \\ \dfrac{1}{6\pi\eta\tilde{a}_{ij}}\left(1 - \dfrac{3|x_i - x_j|}{16\tilde{a}_{ij}}\right) & \\ \qquad (i \neq j \text{ and } |x_i - x_j| < a_i + a_j) & \end{cases}. \tag{5}$$

The last expression is used when the spheres overlap each other, and we employ $\tilde{a}_{ij} = (a_i + a_j)/2$ for the effective Stokes radius.[18] Although this is not the unique form of the effective Stokes radius,[18–20] the above choice is sufficient for our simulation because the motion of the microswimmer is restricted to a one-dimensional space.

3. Simulation Method

The above coupled stochastic differential equations are multiplicative because the noise amplitudes depend on the particle positions. To solve such Langevin equations numerically, we use the Itô interpretation $x_i^* = x_i(t)$ and integrate the quantities[14,15]

$$dx_i = M_{ij}(x^*)f_j(x^*)\,dt + k_{\mathrm{B}}T\frac{\partial M_{ij}(x^*)}{\partial x_j}\,dt + \sqrt{2k_{\mathrm{B}}T\Lambda_{k\ell}(x^*)}Q_{ik}(x^*)(Q^{-1})_{\ell j}(x^*)\,dW_j, \tag{6}$$

where $dW_j \sim \sqrt{dt}$ is the increment of a Wiener process and $\Lambda_{ij} = (Q^{-1})_{ik}M_{k\ell}Q_{\ell j}$ is the diagonalized matrix [$(Q^{-1})_{ij}$ being the inverse matrix of Q_{ij}]. The second term (proportional to $k_{\mathrm{B}}T$) on the right-hand side of Eq. (6) guarantees the equilibrium distribution and is also required for nonequilibrium situations.[14,15]

It should be noted that both of the mobility matrices M_{ij}^{O} and M_{ij}^{RPY} are not positive definite. Hence, we terminate the simulation when the eigenvalue of $\Lambda_{k\ell}$ becomes negative because we need to take its square root in Eq. (6). In the actual simulations, such a situation occurred only for M_{ij}^{O} when a_i is large and the distances between the spheres $|x_i - x_j|$ become small. (More details are explained in the caption of Fig. 2.) In the case of M_{ij}^{RPY}, on the other hand, we did not encounter such a situation and all the simulation runs were completed without any termination.

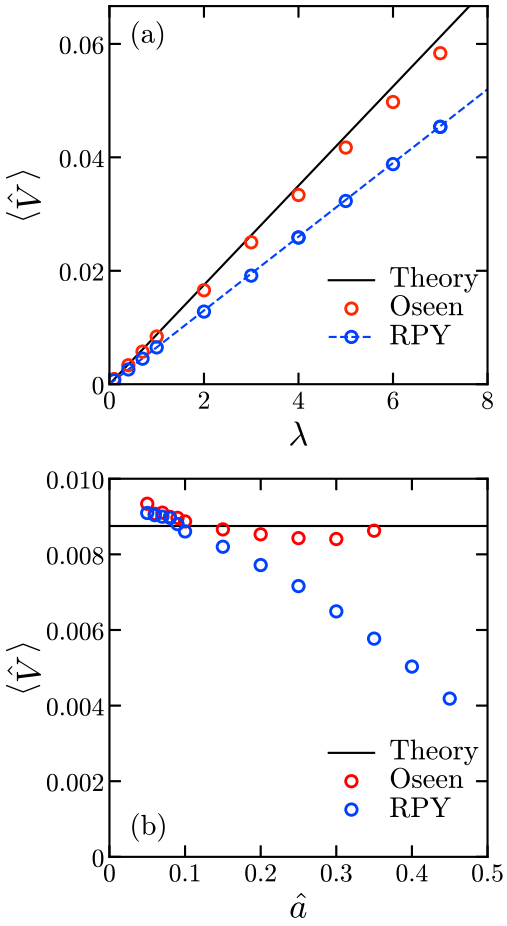

Fig. 2. (Color online) (a) Plot of the the dimensionless average velocity $\langle \hat{V} \rangle = \langle V \rangle \tau/\ell$ ($\tau = 6\pi\eta\ell/K^{\mathrm{e}}$) as a function of $\lambda = K^{\mathrm{o}}/K^{\mathrm{e}}$ when $\hat{a} = 0.3$. (b) Plot of $\langle \hat{V} \rangle$ as a function $\hat{a} = a/\ell$ when $\lambda = 1$. In (a) and (b), the dimensionless temperature is $\hat{T} = k_{\mathrm{B}}T/(K^{\mathrm{e}}\ell^2) = 0.01$, and the black lines are the asymptotic expression in Eq. (4). The red and blue circles are the simulation results obtained by using the Oseen-type [see Eq. (3)] and the RPY-type [see Eq. (5)] mobilities, respectively. The blue dashed line in (a) is the linear fitting to the result of RPY mobility. For the Oseen-type mobility in (b), the ratio of the terminated simulation runs are 0% for $\hat{a} < 0.3$, 0.1% for $\hat{a} = 0.3$, 23% for $\hat{a} = 0.35$, and 100% for $\hat{a} \geq 0.4$ (not plotted).

We scale all the lengths by ℓ and use the spring relaxation time $\tau = 6\pi\eta\ell/K^{\mathrm{e}}$ to make the time dimensionless, i.e., $\hat{t} = t/\tau$. The dimensionless time increment is chosen as $d\hat{t} = 0.001$ for $\lambda \leq 1$ and $d\hat{t} = 0.0001$ for $\lambda > 1$. The simulations were performed for two different dimensionless temperatures, i.e., $\hat{T} = k_{\mathrm{B}}T/(K^{\mathrm{e}}\ell^2) = 0.01$ and 0.001. Each run consists of 10^7 updates of the sphere positions. To calculate the average velocity $\langle V \rangle$, we have taken the average over 2×10^3 and 4×10^3 independent runs for equal and different sphere size cases, respectively.

4. Simulation Results

4.1 Equal sphere size

We first discuss when the sphere size is identical and given by $\hat{a} = a/\ell$. In Fig. 2(a), we plot the dimensionless average velocity $\langle \hat{V} \rangle = \langle V \rangle \tau/\ell$ as a function of $\lambda = K^{\mathrm{o}}/K^{\mathrm{e}}$ when $\hat{a} = 0.3$ and $\hat{T} = 0.01$. The black straight line is the scaled

asymptotic expression in Eq. (4), $\langle \hat{V} \rangle = 7\hat{T}\lambda/8$, whereas the red and blue circles are the simulation results obtained by using the Oseen-type (M_{ij}^{O}) and the RPY-type (M_{ij}^{RPY}) mobilities, respectively. For the Oseen-type mobility, the simulation result agrees well with the asymptotic expression except for larger λ values which give slightly smaller $\langle \hat{V} \rangle$. This result confirms the validity of Eq. (4) for the above parameters. For the RPY-type mobility, on the other hand, the simulation result is systematically smaller than Eq. (4) although the linear dependence on λ is still maintained. This is indicated by the fitted blue dashed line that has a smaller slope. The reason for smaller $\langle V \rangle$ is that the inter-sphere interaction for M_{ij}^{RPY} is generally weaker than that for M_{ij}^{O}. Notice that, in the analytical derivation of Eq. (4), we have used the condition $\hat{a} \ll 1$ while λ does not necessarily have to be small.

In Fig. 2(b), we plot the average velocity $\langle \hat{V} \rangle$ as a function of the sphere size $\hat{a}$ when $\lambda = 1$ and $\hat{T} = 0.01$. According to Eq. (4), $\langle V \rangle$ does not depend on the sphere size a as shown by the black line. For the Oseen-type mobility (red circles), the simulation result is relatively in good agreement with the asymptotic expression up to $\hat{a} \leq 0.35$. When $\hat{a} > 0.4$, however, the mobility matrix is no longer positive definite and most of the simulation runs were terminated. (This is why there is no red data plotted for $\hat{a} \geq 0.4$ for the Oseen-type mobility. The ratio of terminated simulation runs for $\hat{a} \leq 0.35$ is written in the caption of Fig. 2.) For the RPY-type mobility (blue circles), the simulation result coincides with the asymptotic expression up to $\hat{a} \leq 0.15$. For $\hat{a} \geq 0.2$ the simulation data systematically deviates from the asymptotic value and the deviation is more pronounced for larger spheres.

When we reduce the temperature to $\hat{T} = 0.001$, the average velocity discussed above simply decreases by ten times. This is consistent with the fact that $\langle \hat{V} \rangle$ is proportional to $\hat{T}$ in Eq. (4). Since the λ- and $\hat{a}$-dependencies are essentially the same, we do not show the results for $\hat{T} = 0.001$.

Table I. Dimensionless average velocity $\langle \hat{V} \rangle$ when the sphere sizes are different but satisfy the condition $(\hat{a}_1 + \hat{a}_2 + \hat{a}_3)/3 = 0.2$. The combinations of the dimensionless sphere radii are represented by $\hat{a}_1$–$\hat{a}_2$–$\hat{a}_3$. We use the RPY-type mobility for all the cases and the other parameters are $\lambda = 1$ and $\hat{T} = 0.01$. In case (A), we further impose the condition $\hat{a}_1 = \hat{a}_3$ (fore-aft symmetric microswimmers), whereas all the spheres have different sphere size in case (B) (fore-aft asymmetric microswimmers). The range of the numerical error for $\langle \hat{V} \rangle$ is $\pm 0.08 \times 10^{-3}$.

	$\hat{a}_1$–$\hat{a}_2$–$\hat{a}_3$	$\langle \hat{V} \rangle \times 10^3$	$\hat{a}_1$–$\hat{a}_2$–$\hat{a}_3$	$\langle \hat{V} \rangle \times 10^3$
(A)	0.275–0.05–0.275	2.24	0.175–0.25–0.175	7.42
	0.25–0.1–0.25	4.73	0.15–0.3–0.15	6.14
	0.225–0.15–0.225	6.72	0.125–0.35–0.125	4.36
	0.2–0.2–0.2	7.68	0.1–0.4–0.1	2.62
(B)	0.2–0.1–0.3	4.52	0.3–0.1–0.2	4.69
	0.1–0.2–0.3	5.88	0.3–0.2–0.1	5.97
	0.1–0.3–0.2	5.38	0.2–0.3–0.1	5.47

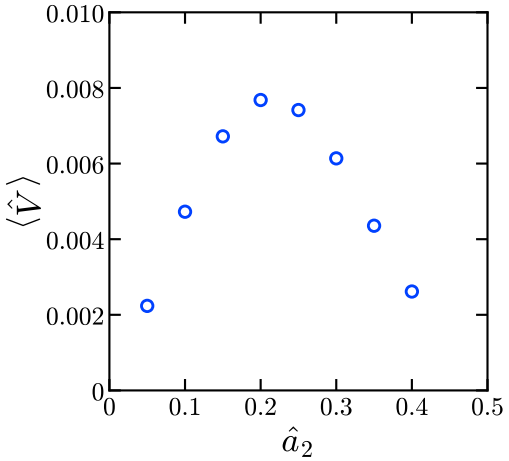

Fig. 3. (Color online) Plot of the the dimensionless average velocity $\langle \hat{V} \rangle$ as a function of the middle sphere size $\hat{a}_2$ for the case (A) in Table I. For comparison, we impose the conditions $(\hat{a}_1 + \hat{a}_2 + \hat{a}_3)/3 = 0.2$ and $\hat{a}_1 = \hat{a}_3$ (fore-aft symmetric microswimmers).

4.2 Different sphere size

Next, we discuss the cases when the sphere sizes are different. This is currently possible only by performing simulations because there is no corresponding analytical prediction. In order to make fair comparisons, we investigate several cases for which the average sphere size is always fixed to $(\hat{a}_1 + \hat{a}_2 + \hat{a}_3)/3 = 0.2$. We use the RPY-type mobility for all the cases and the parameters are set to $\lambda = 1$ and $\hat{T} = 0.01$ as before. The simulation results of the average velocity $\langle \hat{V} \rangle$ are summarized in Table I. For the case (A), we further impose the condition $\hat{a}_1 = \hat{a}_3$ and vary the middle sphere size $\hat{a}_2$ (fore-aft symmetric microswimmers). For the case (B), on the other hand, all the spheres have different sphere size (fore-aft asymmetric microswimmers).

In Fig. 3, we plot $\langle \hat{V} \rangle$ as a function of the middle sphere size $\hat{a}_2$ for the case (A) in Table I. Within this comparison, we clearly see that $\langle \hat{V} \rangle$ takes the largest value when all the spheres have the same size, i.e., $\langle \hat{V} \rangle \approx 7.68 \times 10^{-3}$ when 0.2–0.2–0.2. Hence, for the fore-aft symmetric microswimmers, the size of the middle sphere essentially determines their average velocity.

For the fore-aft asymmetric microswimmers in case (B), on the other hand, we first note that $\langle \hat{V} \rangle$ is always smaller than that of the equal size case, i.e., 0.2–0.2–0.2. It is interesting to note that $\langle \hat{V} \rangle$ almost coincides (within the error bars) between the two asymmetric microswimmers such as 0.1–0.2–0.3 and 0.3–0.2–0.1. (However, such a quantitative coincidence may not hold between 0.2–0.1–0.3 and 0.3–0.1–0.2.) Even for these fore-aft asymmetric microswimmers, the size of the middle sphere $\hat{a}_2$ plays an important role and the behavior of $\langle \hat{V} \rangle$ is similar to Fig. 3. The average velocity takes the largest and the smallest values for $\hat{a}_2 = 0.2$ and 0.1, respectively.

The decrease of $\langle \hat{V} \rangle$ for the different sphere size cases can be physically understood in the following way. In general, the change in the average velocity can be attributed to both active and passive origins. Within the comparison in Fig. 3, the overall hydrodynamic friction is similar because the average sphere size has been fixed, leading to the similar passive contribution. The fact that $\langle \hat{V} \rangle$ dramatically reduces both for $\hat{a}_2 \gg \hat{a}_1 = \hat{a}_3$ (effectively one sphere) and $\hat{a}_2 \ll \hat{a}_1 = \hat{a}_3$ (effectively two spheres) is that the internal actuation due to odd elasticity does not operate efficiently for these cases. Hence the drop of $\langle \hat{V} \rangle$ in Fig. 3 can be mainly explained by the lack of internal active drive in odd microswimmers having different sphere size.

5. Summary and Discussion

To conclude, we have performed the numerical simulations of the previously proposed odd microswimmers by using both the Oseen-type and the RPY-type mobilities. For the Oseen-type mobility, the simulation results quantitatively reproduce the asymptotic expression of the average velocity. For the RPY-type mobility, on the other hand, the average velocity is smaller than that of the Oseen-type mobility due to the weaker hydrodynamic interactions. Performing simulations for microswimmers having different sphere sizes, we showed that the average velocity becomes smaller than that of the equal size case. Moreover, the size of the middle sphere plays an important role in determining the average velocity for both fore-aft symmetric and antisymmetric microswimmers.

Here, we give a rough estimate of the parameter $\lambda = K^{\mathrm{o}}/K^{\mathrm{e}}$ that is the most important quantity in our model. We consider the case when the concept of odd elasticity is applied to the structural changes of enzymes and motor proteins even though they are usually not microswimmers.[5–7] According to the experiments on a kinesin molecule,[21] the even elasticity can be roughly estimated as $K^{\mathrm{e}} \approx 10^{-4}\,\mathrm{J/m^2}$. On the other hand, the active force due to kinesin is estimated to be $f \approx 10^{-11}\,\mathrm{N}$.[21] By roughly estimating the natural length to be $\ell \approx 10^{-8}\,\mathrm{m}$, the odd elastic constant can be estimated as $K^{\mathrm{o}} \sim f/\ell \approx 10^{-3}\,\mathrm{J/m^2}$. Then the ratio between the odd and even elastic constants is typically $\lambda = K^{\mathrm{o}}/K^{\mathrm{e}} \approx 10$. This is consistent with the plotted range of λ Fig. 2(a). [Notice again that λ in Eq. (4) does not necessarily have to be small.]

Even though odd microswimmers are not yet realized experimentally, the concept of odd elasticity has been employed in odd active robots.[22,23] We believe that the results of the current simulations will be useful in designing odd microswimmers in the future.

Acknowledgment We thank K. Ishimoto for useful discussions. K.Y. acknowledges the support by a Grant-in-Aid for JSPS Fellows (No. 21J00096) from the Japan Society for the Promotion of Science (JSPS). S.K. acknowledges the support by the National Natural Science Foundation of China (Nos. 12274098 and 12250710127) and the startup grant of Wenzhou Institute, University of Chinese Academy of Sciences (No. WIUCASQD2021041).

*komura@wiucas.ac.cn

1) C. Scheibner, A. Souslov, D. Banerjee, P. Surówka, W. T. M. Irvine, and V. Vitelli, Nat. Phys. **16**, 475 (2020).
2) M. Fruchart, C. Scheibner, and V. Vitelli, arXiv:2207.00071.
3) L. Braverman, C. Scheibner, B. VanSaders, and V. Vitelli, Phys. Rev. Lett. **127**, 268001 (2021).
4) T. H. Tan, A. Mietke, J. Li, Y. Chen, H. Higinbotham, P. J. Foster, S. Gokhale, J. Dunkel, and N. Fakhri, Nature **607**, 287 (2022).
5) K. Yasuda, K. Ishimoto, A. Kobayashi, L.-S. Lin, I. Sou, Y. Hosaka, and S. Komura, J. Chem. Phys. **157**, 095101 (2022).
6) K. Yasuda, A. Kobayashi, L.-S. Lin, Y. Hosaka, I. Sou, and S. Komura, J. Phys. Soc. Jpn. **91**, 015001 (2022).
7) A. Kobayashi, K. Yasuda, K. Ishimoto, L.-S. Lin, I. Sou, Y. Hosaka, and S. Komura, arXiv:2211.16089.
8) E. M. Purcell, Am. J. Phys. **45**, 3 (1977).
9) M. Doi, *Soft Matter Physics* (Oxford University Press, Oxford, U.K., 2013).
10) L.-S. Lin, K. Yasuda, K. Ishimoto, Y. Hosaka, and S. Komura, J. Phys. Soc. Jpn. **92**, 033001 (2023).
11) K. Yasuda, Y. Hosaka, I. Sou, and S. Komura, J. Phys. Soc. Jpn. **90**, 075001 (2021).
12) J. Rotne and S. Prager, J. Chem. Phys. **50**, 4831 (1969).
13) H. Yamakawa, J. Chem. Phys. **53**, 436 (1970).
14) A. W. C. Lau and T. C. Lubensky, Phys. Rev. E **76**, 011123 (2007).
15) T. Kuroiwa and K. Miyazaki, J. Phys. A **47**, 012001 (2014).
16) R. Golestanian and A. Ajdari, Phys. Rev. E **77**, 036308 (2008).
17) R. Golestanian, Eur. Phys. J. E **25**, 1 (2008).
18) B. Carrasco, J. G. de la Torre, and P. Zipper, Eur. Biophys. J. **28**, 510 (1999).
19) E. Wajnryb, K. A. Mizerski, P. J. Zuk, and P. Szymczak, J. Fluid Mech. **731**, R3 (2013).
20) P. J. Zuk, E. Wajnryb, K. A. Mizerski, and P. Szymczak, J. Fluid Mech. **741**, R5 (2014).
21) T. Ariga, M. Tomishige, and D. Mizuno, Phys. Rev. Lett. **121**, 218101 (2018).
22) K. Ishimoto, C. Moreau, and K. Yasuda, Phys. Rev. E **105**, 064603 (2022).
23) M. Brandenbourger, C. Scheibner, J. Veenstra, V. Vitelli, and C. Coulais, arXiv:2108.08837.